Propagation Lengths and Group Velocities of Plasmons in Chemically Synthesized Gold and Silver Nanowires

Barbara Wild,[†] Lina Cao,[†,‡] Yugang Sun,[‡] Bishnu P. Khanal,[§] Eugene R. Zubarev,[§] Stephen K. Gray,[‡] Norbert F. Scherer,[†,‡] and Matthew Pelton[‡,*]

[†]Department of Chemistry and The James Franck Institute, The University of Chicago, 929 East 57th Street, Chicago, Illinois 60637, United States, [‡]Center for Nanoscale Materials, Argonne National Laboratory, 9700 South Cass Avenue, Argonne, Illinois 60439, United States, and [§]Department of Chemistry, Rice University, 6100 Main Street, Houston, Texas 77005, United States

ABSTRACT Recent advances in chemical synthesis have made it possible to produce gold and silver nanowires that are free of large-scale crystalline defects and surface roughness. Surface plasmons can propagate along the wires, allowing them to serve as optical waveguides with cross sections much smaller than the optical wavelength. Gold nanowires provide improved chemical stability as compared to silver nanowires, but at the cost of higher losses for the propagating plasmons. In order to characterize this trade-off, we measured the propagation length and group velocity of plasmons in both gold and silver nanowires. Propagation lengths are measured by fluorescence imaging of the plasmonic near fields. Group velocities are deduced from the spacing of fringes in the spectrum of coherent light transmitted by the wires. In contrast to previous work, we interpret these fringes as arising from a far-field interference effect. The measured propagation characteristics agree with numerical simulations, indicating that propagation in these wires is dominated by the material properties of the metals, with additional losses due to scattering from roughness or grain boundaries providing at most a minor contribution. The propagation lengths and group velocities can also be described by a simple analytical model that considers only the lowest-order waveguide mode in a solid metal cylinder, showing that this single mode dominates in real nanowires. Comparison between experiments and theory indicates that widely used tabulated values for dielectric functions provide a good description of plasmons in gold nanowires but significantly overestimate plasmon losses in silver nanowires.

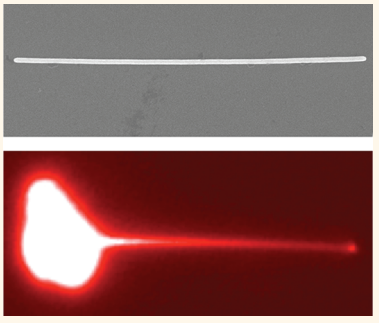

KEYWORDS: surface plasmons · nanowires · propagation length · group velocity

Surface plasmons (SPs) are electromagnetic waves bound to free-electron oscillations at the surface of a metal.[1] Light at visible and near-infrared frequencies can couple to SPs in gold and silver nanostructures, resulting in the concentration of optical fields to dimensions well below the optical wavelength. Plasmonic metal structures can thus be the basis of nanophotonic devices that are much smaller than conventional optical circuits.[2] The simplest such device is a plasmonic waveguide, which serves to transport optical signals between different components.[3,4] The central goal in constructing nanophotonic waveguides is simultaneously achieving high-speed and low-loss data transmission or image transfer[5] and confinement of the optical fields to dimensions much smaller than the diffraction limit.

The simplest plasmonic waveguide is a solid nanowire of silver or gold. Experimental studies of such waveguides initially focused on strips of metal fabricated using metal evaporation and electron-beam lithography.[6−10] Although these structures are capable of supporting propagating plasmons, the plasmons suffer significant losses due to scattering off the rough surfaces and grain boundaries that are inherent to these lithographically fabricated structures. Colloidal synthesis has been demonstrated as an inexpensive route for the bottom-up fabrication of silver nanowires without grain boundaries and with very smooth surfaces,[11] and low-loss propagation of plasmons has been observed in such nanowires.[11,12] However, silver is chemically unstable under ambient conditions, readily reacting with oxygen and hydrogen sulfide in the environment. Chemically synthesized silver nanowires thus generally have a lifetime of only about one day when exposed to the atmosphere and must be carefully protected if they are to be used.

Gold, by contrast, is more chemically stable in ambient conditions. Early attempts to fabricate single-crystal gold wires involved labor-intensive methods such as nanoskiving.[13] Recently, though, it has been demonstrated that colloidal synthesis methods can be used to fabricate gold

* Address correspondence to pelton@anl.gov.

Received for review October 4, 2011 and accepted December 20, 2011.

Published online December 20, 2011
10.1021/nn203802e

nanowires with high aspect ratios and structural properties similar to those of the silver nanowires.[14,15] In particular, the gold and silver nanowires both have pentagonal cross sections and have diameters around 100 nm for lengths in the range from 10 to 20 μm. The high quality of these wires has been demonstrated to lead to dc conductivities near the bulk limiting value.[15] Plasmon propagation has been observed for a wavelength of 532 nm in chemically synthesized gold nanowires with large diameters.[16] For these short wavelengths, the optical absorption of gold is strong due to interband absorption, and the SPs can propagate only very short distances before being absorbed. At longer wavelengths, which are more relevant for applications, it is expected that the losses will be less severe and the propagation lengths will thus be longer.

Shorter propagation lengths are nonetheless expected at all wavelengths in gold nanowires as compared to silver.[17] It is therefore important to quantify these propagation lengths, in order to determine the trade-off that is being made in exchange for the improved chemical and physical stability of the gold nanowires. As well as losses, dispersion will limit the application of nanowires as plasmonic interconnects. Together, dispersion and loss as a function of frequency provide a complete description of propagation in waveguides, and a quantitative determination of these values is necessary if they are to be used as nanophotonic interconnects.

Dispersion and loss are often described using complex propagation constants or effective refractive indices. Experimentally, it is more convenient to use the propagation length, L_{prop}, and the group velocity, v_{gr}. The propagation length is defined as the energy decay length for plasmons propagation along the wires; that is, the intensity of the SP field at a point x along the propagation direction is given by

$$I_{SP} = I_0 e^{-x/L_{prop}} \quad (1)$$

The group velocity is defined as the derivative of the dispersion relation

$$v_{gr} = \frac{d\omega}{dk_{SP}} \quad (2)$$

where ω is the angular frequency and k_{SP} is the wavenumber of the SP propagating along the nanowire. Although v_{gr} describes dispersion only within an overall phase factor, it defines the speed at which signals travel along the waveguide and is thus the crucial quantity when using the nanowires as plasmonic interconnects. The propagation length and group velocity are characteristics of the waveguide modes that are excited in the nanowires; they therefore depend on the cross section of the nanowire but are independent of its length or how the modes are excited.

In this paper, we experimentally quantify the propagation length and group velocity for SPs in chemically synthesized gold and silver nanowires.[14,18] In addition, we provide a simple theoretical description of the propagation that will facilitate application of these nanowires as plasmonic waveguides. First, using rigorous electrodynamic simulations, we demonstrate that propagation in the nanowires is dominated by the dielectric functions of the metals, with additional losses due to defects providing at most a minor contribution. In fact, the propagation is so good that well-regarded measurements of the dielectric function (in ref 17) are inadequate to describe the plasmon losses in silver; that is, the losses we measure are less than what are generally considered to be minimum possible values. Furthermore, we show that the propagation characteristics can be described quantitatively by a simple analytical model for the lowest-order waveguide mode in a solid metal cylinder. Finally, we identify far-field interference as the origin of the observed fringes in the output spectrum of the nanowires when they are excited by broad-band, coherent light, in contrast to other reports of the spectroscopic properties of metal nanowires.

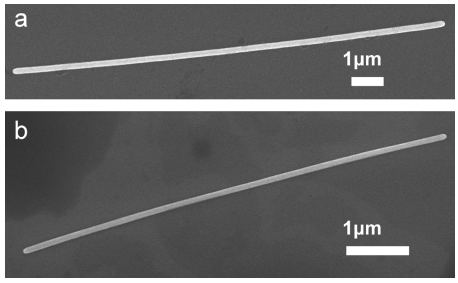

Figure 1. Scanning electron microscope images of chemically synthesized (a) gold and (b) silver nanowires. Here the nanowires were deposited on a silicon substrate to allow scanning electron microscopy.

RESULTS

Plasmon Propagation Length. Scanning electron microscope (SEM) images of representative gold and silver nanowires are shown in Figure 1. The nanowires have lengths up to 14 μm and diameters, D, of about 120 nm for the gold wires and 80 nm for the silver wires. As a first step to fully characterize the properties of SPs propagating in gold and silver nanowires, we measured the propagation length of the SPs. The method used is based on the ability of the propagating SPs to excite fluorescence of dye molecules that are in close proximity to the nanowire through the evanescent fields that extend from the metal surfaces.[19,20]

The nanowires are deposited on a glass substrate and embedded in a thin layer of poly(methyl methacrylate) (PMMA) containing fluorescent dye molecules. As well as holding the dye molecules, the PMMA layer serves to protect the silver nanowires against degradation. In addition, the PMMA has nearly the same refractive index as the glass substrate, so that

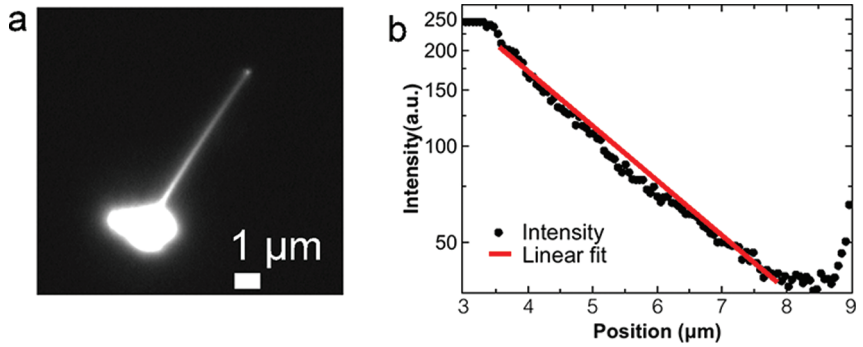

Figure 2. (a) Image of two-photon fluorescence excited by surface plasmons propagating along a silver nanowire. (b) Two-photon fluorescence intensity, obtained from the image, as a function of the position along the nanowire. Points are experimental data; red line is exponential fit (linear fit on logarithmic scale).

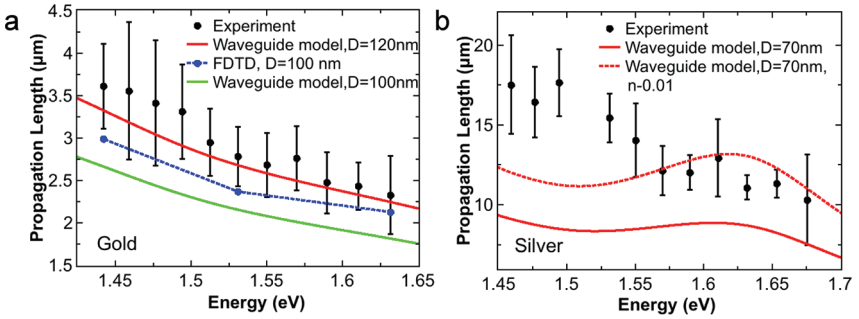

Figure 3. Propagation lengths as a function of energy for surface plasmons propagating along (a) gold and (b) silver nanowires. Black points are average values from measurements; error bars are standard deviation. Blue points and blue dashed line: values calculated using finite-difference time-domain simulations for a nanowire with a diameter of 100 nm. Solid curves: values obtained from a waveguide model. For gold wires, the green curve shows values for a nanowire diameter of 100 nm, and the red curve for 120 nm. For silver wires, the red curve shows values for a diameter of 70 nm. Red dashed curve: values for a diameter of 70 nm, calculated by uniformly decreasing the real part of the refractive index for silver by 0.01 from tabulated values in ref 17.

the nanowires experience a homogeneous dielectric environment. One end of the nanowire is excited with a focused laser beam in an optical microscope; some of the light scattered off the end of the wire is coupled into SPs that propagate along the wire. These propagating SPs excite two-photon fluorescence from dye molecules in their optical near field. This fluorescence is imaged using the same optical microscope onto a CCD camera, producing images such as the one shown in Figure 2a. The fluorescence intensity in this image decays exponentially, as shown in Figure 2b; because two-photon fluorescence is used for imaging, the decay length of the fluorescence is half the plasmon propagation length:

$$I_{\text{fluor}} \sim (I_{\text{SP}})^2 = I_0^2 e^{-2x/L_{\text{prop}}} \quad (3)$$

Fluorescence images were obtained and propagation lengths determined by fitting the fluorescence decay for a range of laser frequencies for individual gold and silver wires. The experimental results are summarized in Figure 3, with the points showing the average values and the error bars showing the standard deviations associated with the measured results from four wires. This distribution of propagation lengths is related to the distribution of nanowire diameters in the sample since, as we show below, the propagation length decreases as the diameter decreases.

In the case of the gold nanowires, we measured propagation lengths in the range of 2.4 to 3.6 μm for the photon energy range of 1.44 to 1.63 eV; *i.e.*, wavelengths of 760 to 860 nm (Figure 3a). The measured propagation lengths are greater than previous reported values for thin gold strip waveguides, reflecting the substantial reduction and perhaps even absence of scattering from grain boundaries and surface roughness in our chemically synthesized nanowires. The propagation length reported in ref 16 of about 1.8 μm at a photon energy of 2.3 eV is consistent with an extrapolation of our results. By contrast, the propagation lengths determined for the silver nanowires are greater, due to the lower optical losses in silver as compared to gold, ranging from 11 to 17.5 μm over the measured frequency range (Figure 3b). These results are consistent with a previously measured propagation length of about 10 μm at a photon energy of 1.58 eV[11] but are much greater than a previous report of a 3 μm propagation length for a photon energy of 1.5 eV.[21] Other measurements have involved photon energies outside of the range that we measure[20−23] but are consistent with an extrapolation of our results. A quantitative

TABLE 1. Calculated and Measured Plasmon Propagation Lengths in Gold Nanowires

	plasmon propagation length, L_{prop} (μm)			
	waveguide model		FDTD calculation	experiment
photon energy (eV)	D = 120 nm	D = 100 nm	D = 100 nm	
1.63	2.3	1.8	2.1	2.3
1.53	2.7	2.2	2.4	2.8
1.44	3.3	2.7	3.0	3.6

comparison to these previous results is not possible, though, because the nanowires that were previously measured have, in general, different diameters than those considered here, and the exact diameters were not always reported. Similarly, longer propagation lengths have been measured in other geometries, including smooth films,[24] but these have not be obtained at the same time as two-dimensional confinement well below the diffraction limit, as in the nanowires.

In order to understand the measured propagation lengths, we modeled plasmon propagation in gold nanowires with finite-difference time-domain (FDTD) numerical simulations.[25,26] In these calculations, a radiating point dipole with a particular frequency (corresponding to a particular photon energy) was placed at one end of the nanowire, exciting propagating plasmons in the wire. The gold nanowire diameter was taken to be 100 nm, equal to the average of diameters measured from SEM images such as those shown in Figure 1. Since the dielectric constants of PMMA and glass are nearly identical, the simulations treat the wire as being surrounded by a homogeneous dielectric environment. An exponential fit to the decaying electric-field intensity along the wire then gives the corresponding SP propagation length. The calculation results, as shown in Figure 3a and Table 1, track the measured values well but are consistently lower by approximately 0.25 μm; part of this difference may be attributable to the relatively large grid size required for the FDTD calculations. The fact that the measured propagation lengths are as long as, or even longer than, predicted by the calculations demonstrates that the plasmon losses in these wires are dominated by intrinsic losses in the metal, with scattering providing at most a minor contribution to the propagation losses.

Because of the long lengths of the nanowires, the FDTD calculations are computationally expensive. Nevertheless, we can use the good agreement of experiment and FDTD simulations to establish the veracity of an analytical model that provides a simpler description of the SP propagation and allows for greater physical insight into their characteristics. For this model, we consider the waveguide modes of an infinitely long, solid cylindrical rod with a circular cross section. In particular, we consider only the lowest-order waveguide mode, which satisfies the following characteristic equation:[27,28]

$$\frac{\varepsilon(\omega)}{KR}\frac{J_1(KR)}{J_0(KR)} - \frac{\varepsilon_S}{K_S R}\frac{H_1^{(1)}(K_S R)}{H_0^{(1)}(K_S R)} = 0 \qquad (4)$$

with

$$K^2 = \varepsilon(\omega)\omega^2/(c^2 - h^2) \qquad (5a)$$

and

$$K_S^2 = \varepsilon_S\omega^2/(c^2 - h^2) \qquad (5b)$$

where $J(x)$ and $H(x)$ are ordinary Bessel functions and Hankel functions, respectively, $R = D/2$ is the radius of the wire, $\varepsilon(\omega)$ is the complex dielectric function of the metal, ε_S is the dielectric constant of the surrounding medium, ω is the optical frequency, c is the speed of light in the vacuum, and h is the complex propagation constant for the waveguide mode:

$$h = k_{SP} + i\alpha \qquad (6)$$

where $L_{prop} = 1/(2\alpha)$. The group velocity can be calculated as $v_{gr} = 1/(\partial k_{SP}/\partial\omega)$.

In our experiments, the nanowires are surrounded by PMMA and glass, providing a nearly homogeneous dielectric environment with $\varepsilon_S = 2.25$. The silver and gold dielectric constants are taken from ref 17. We use a simulated annealing procedure[29] to find the real, positive values of α and k_{SP} that satisfy eq 4. An important point concerns the branch adopted for $K_S = (\varepsilon_S\omega^2/(c^2 - h^2))^{1/2}$: the sign must be chosen such that $\mathrm{Im}[K_S] > 0$ because only then are Hankel functions of the first kind asymptotically stable and thus valid cylindrical wave functions.

Figure 3a shows the calculated propagation lengths, according to the waveguide model described above, for a gold nanowire with a diameter of 100 nm. There is only a small offset, approximately 0.25 μm, between the waveguide model and FDTD results, indicating that the model captures the essential physics of the problem. Compared to the experimental results, the waveguide model gives values that are consistently lower by 0.5−0.75 μm. The offset can be partially attributed to the choice of the diameter for the circular cross section of the waveguide: (i) both calculations approximate the pentagonal nanowire cross section as circular, and the proper choice of diameter in the model is not obvious; (ii) it is difficult to obtain a precise measurement of the nanowire diameter from SEM images; and (iii) nanowires in the sample have a distribution of diameters, with wires observed in the SEM having apparent diameters that range from 90 to 170 nm. It is therefore reasonable to treat the waveguide diameter as a fitting parameter when comparing theory to experiment. With this single adjustable parameter, we are able to achieve quantitative agreement between the calculated and measured propagation

TABLE 2. Calculated and Measured Plasmon Propagation Lengths in Silver Nanowires

	plasmon propagation length, L_{prop} (μm)							
	dielectric function ref 17				dielectric function ref 30			
	waveguide model			FDTD	waveguide model		FDTD	
photon energy (eV)	D = 70 nm	D = 70 nm (n − 0.01)	D = 90 nm	D = 90 nm	D = 70 nm	D = 90 nm	D = 90 nm	experiment
1.67	7.6	11.1	10.8		1.4	2.0		10.3
1.58	8.8	12.8	12.2	11	1.7	2.4	2.2	12
1.46	9.2	12	12.7		2.1	3.0		17.5

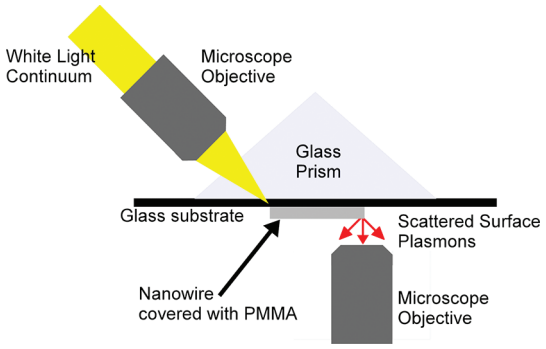

Figure 4. Sketch of the experimental setup for the measurement of group velocity for surface plasmons in metal nanowires (not to scale).

lengths in gold nanowires, as shown in Figure 3a and Table 1. We note that, as shown later, the same value of 120 nm for the nanowire diameter that reproduces the measured propagation lengths also allows for quantitative agreement with measured group velocities in the nanowires. (A similar optimization would, in principle, be possible using FDTD calculations but would be computationally prohibitive.)

For silver nanowires, the agreement with the waveguide model is much poorer, even if the nanowire diameter is used as an adjustable parameter. Figure 3b and Table 2 show the results of waveguide calculations for a silver nanowire with a diameter of 70 nm, which was also optimized with respect to the measured group velocities. The fitted diameter compares reasonably to a measured range of 60−100 nm from SEM images. In addition, the waveguide model gives propagation lengths in reasonable agreement with FDTD calculations, as shown in Table 2. We therefore attribute the disagreement between the model and the experiment, not to any flaw in the model itself, but rather to inaccuracies in the tabulated values of the dielectric function. The propagation length is sensitive principally to the imaginary part of the dielectric function of silver, $\mathrm{Im}[\varepsilon] = 2nk$, where n and k are the corresponding real and imaginary parts of the refractive index. In the photon energy range considered, the magnitude of n is small, so that experimental uncertainties in tabulated values are significant and can lead to considerable uncertainty in $\mathrm{Im}[\varepsilon]$. For example, at $\hbar\omega$ = 1.64 eV, $n = 0.03 \pm 0.02$, according to ref 17. Simply reducing n by 0.01 from tabulated values, which is well within the reported experimental error, leads to significantly different values for the calculated propagation, as shown in Figure 3b and Table 2. Table 2 also shows that using different tabulated values for the dielectric constant of silver, such as those in ref 30, leads to calculated propagation lengths that do not at all agree with experimental values.

We note also that, since the imaginary parts of the dielectric functions are larger in gold than in silver, the errors in these tabulated values have less of an impact on the calculated propagation lengths for gold wires; the experimental uncertainties in ref 17, for example, correspond to errors of only 12% in calculated propagation lengths in gold nanowires. Regardless of the values chosen for the dielectric constant, the measured propagation lengths in the silver nanowires are consistently longer than or equal to the calculated values, again indicating that extrinsic losses such as surface scattering are negligible in these chemically synthesized nanowires.

Plasmon Group Velocity. Apart from the propagation length, the key quantity describing propagation in waveguides is the group velocity. In order to determine v_{gr} in the gold and silver nanowires, they were excited by a white-light continuum focused on one end of the nanowire (which we refer to as the input) in a total internal reflection configuration (Figure 4). The excited SPs propagate to the other end of the nanowire (which we refer to as the output), where they scatter into the far field. The output light is imaged onto the input slit of a spectrometer, which is used to measure the spectrum of light emerging from the nanowires. The samples were coated with PMMA to protect them against chemical degradation and to provide a homogeneous dielectric environment; unlike for the samples used for the propagation length measurements, no dye molecules are embedded in the PMMA layers.

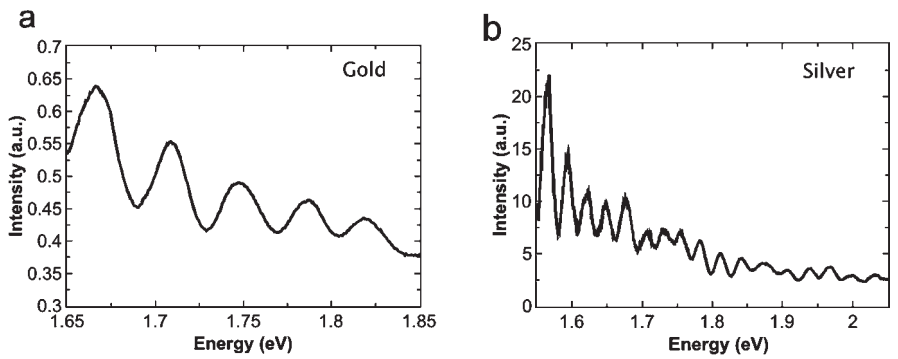

Figure 5. Spectrum of light emerging from the output end of (a) a 10 μm long gold nanowire and (b) a 14 μm long silver nanowire.

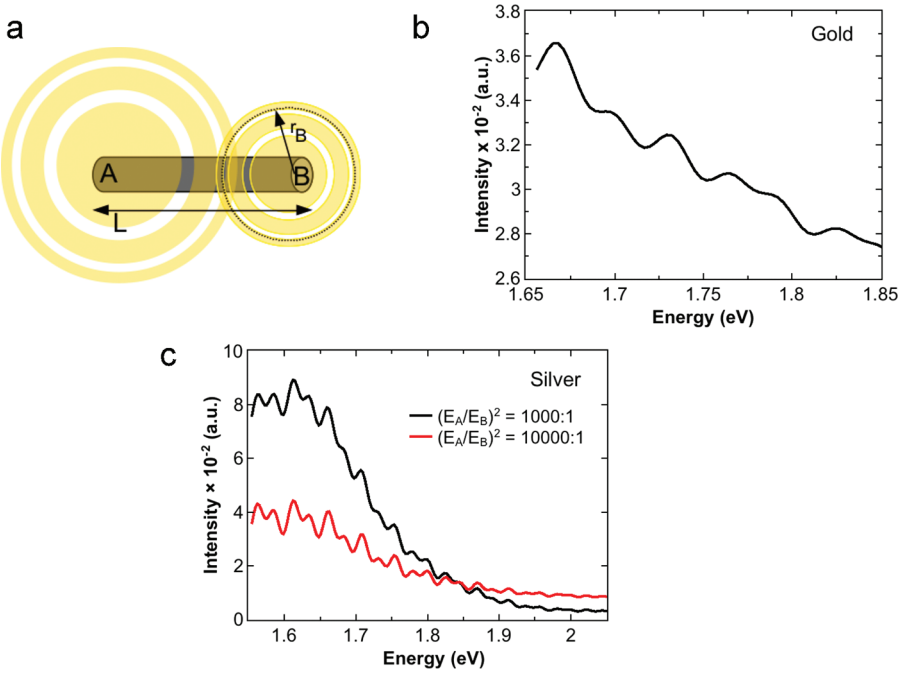

Figure 6. (a) Illustration of the input and output scattering spots on a metal nanowire. Calculated interference between scattered "input" light (A) and the "output" light (B) that propagates along (b) a 10 μm long gold nanowire and (c) a 14 μm long silver nanowire. The calculations are based on eq 7, an idealized model of far-field interference. Results are normalized by arbitrary factors so that they can be plotted on the same *y*-axis.

As shown in Figure 5, the transmission spectra exhibit strong oscillations as a function of frequency. Similar fringes have previously been observed in the output spectrum of silver nanowires and have been interpreted as corresponding to standing waves along the length of the wire, analogous to Fabry-Pérot cavity modes.[11,12] However, theoretical calculations using either the FDTD method[26] or the waveguide model predict that these standing-wave modes would produce a fringe spacing equal to half what is measured. We therefore propose an alternative origin for the spectral fringes that we observe, based on far-field interference between incident light that scatters off the input end of the nanowire and light emerging from the output.

The majority of the light scattered off the input end of the wire is scattered into the far field, and this strong scattering is collected by the microscope objective that is used to collect light from the output end of the wire. Only a small fraction of the scattered input light couples into SPs that propagate along the wire; these SPs are further attenuated by losses along the wire, and only a fraction of the SPs that reach the far end of the wire scatter out to free space and are collected by the objective. The output spot is therefore much less intense than the input spot. In fact, when the output spot is imaged, nearly as much light may be captured from the scattered input light as from the output spot itself. This is confirmed by wide-field optical images on the nanowires, which show a significant optical background at the output end of the wire. Light from the input end of the wire will therefore interfere with light from the output end, producing the observed spectral fringes.

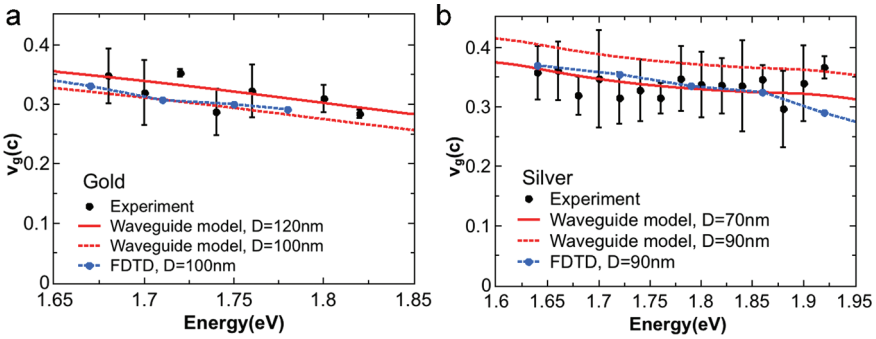

Figure 7. Group velocity as function of energy for surface plasmons propagating along (a) gold and (b) silver nanowires. Black points are average values from measurements; error bars are standard deviation. Blue points: values calculated using finite-difference time-domain simulations; the gold nanowire is taken to have a diameter of 100 nm, and the silver a diameter of 90 nm. Red solid curve: values calculated by a waveguide model; the gold nanowire is taken to have a diameter of 120 nm, and the silver a diameter of 70 nm. Red dashed curve: values calculated by a waveguide model; the gold nanowire is taken to have a diameter of 100 nm, and the silver a diameter of 90 nm.

This far-field interference can be illustrated by considering the idealized case in which the microscope objective used to collect the scattered light forms perfect, diffraction-limited images of both the input and output spots. In this case, the images of the input spot (point A in Figure 6a) and the output spot (point B) can each be described as Airy disks, producing the following electric field at the position (x,y) in the image plane:

$$E(x,y) = E_A \frac{J_1(kr_A\alpha)}{kr_A\alpha} + E_B e^{ik_{SP}L} e^{-L/(2L_{prop})} \frac{J_1(kr_B\alpha)}{kr_B\alpha} \quad (7)$$

where $k = \omega/c$ is the free-space wavenumber of the scattered light, r_A is the distance from (x,y) to point A, r_B is the distance to point B, E_A is the amplitude of the field scattered at point A, E_B is the amplitude scattered at point B, and $\alpha = M \cdot (\mathrm{NA})$, where M is the magnification of the image and NA is the numerical aperture of the objective. The factor $e^{ik_{SP}L}$ takes into account the phase of the SP after traveling once along the length of the wire, L, from point A to point B, and $e^{-L/(2L_{prop})}$ accounts for propagation loss. For this illustration, we use the dispersion relationships inferred from the waveguide calculations in order to approximate k_{SP} and L_{prop}, and we take $E_A^2 = 1000\, E_B^2$, as a reasonable approximation of the experimental condition. The output field is integrated over a circle of radius 1 μm around point B to approximate the area of the sample that is collected in the experiment. Figure 6b,c show the spectra calculated from this model for a Au wire with $L = 10$ μm and a Ag wire with $L = 14$ μm, respectively. The calculated spectra show fringes with nearly the same energy spacing as in the experimental spectra. Figure 6c compares the results for a silver wire with $E_A^2 = 10\,000\, E_B^2$ to those for $E_A^2 = 1000\, E_B^2$, demonstrating that the fringe spacing is not sensitive to the assumed scattering strength.

We note that this model is not intended to provide a quantitative description of the experiment but is rather intended simply to demonstrate that far-field interference can produce fringes in the measured spectra, and that those fringes have the same spacing as the ones we measure experimentally. In particular, it is clear that the idealizations of the model lead to calculated fringes that have lower visibility than those measured experimentally. Despite its approximations, though, the model allows the quantitative prediction that the maxima of a far-field interferogram are determined by the phase accumulated by SPs as they propagate from one end of the wire to the other. Specifically, a fringe maximum means that the light scattered from the input at A and the light emerging from the output at B are in phase with one another. This will occur when the phase accumulated by the SP when propagating from one end of the wire to another is an integer multiple of 2π:

$$\Phi = k_{SP}L = 2\pi m \quad (8)$$

for integer values of m. The fringe spacing can therefore be used to obtain a piecewise estimate of the SP group velocity:

$$v_{gr} \approx \frac{\Delta\omega}{\Delta k_{SP}} = \frac{L\Delta\omega}{2\pi\Delta m} \approx Lc\frac{\Delta\lambda}{\lambda_o^2} \quad (9)$$

where $\Delta\omega$ is the difference in frequency, Δk_{SP} the difference in wavenumber, and $\Delta\lambda$ the difference in wavelength for SPs at two adjacent fringe maxima, for which $\Delta m = 1$, and where λ_o is the center wavelength between the two fringes. It is important to note that eq 8 is different by a factor of 2 from the condition for standing waves along the wire.[12,26] In other words, for a given dispersion relation and a given photon frequency range, the number of fringe maxima predicted by the far-field interference model is exactly half the number of fringe maxima predicted based on the standing-wave resonance condition. This is the key qualitative feature that the model describes that is consistent with the experimental observations.

Figure 7 shows the spectral dependence of the group velocity extracted from scattering spectra of six gold nanowires and eight silver nanowires. The measured group velocities from the different nanowires

were grouped together in energy bins of 0.2 eV, and the average and standard deviation of the measured values are plotted for each of those bins. The group velocity of the gold nanowires decreases monotonically over the measured energy range, reflecting increasing dispersion in the dielectric function of gold as the photon energy approaches the energy of intraband transitions. By contrast, the group velocity of the silver nanowires is nearly constant over the measured range.

These measured group velocities can again be compared to FDTD calculations and to the waveguide model. For FDTD calculations, the wires are excited by a plane wave whose propagation direction is perpendicular to the long axis of the wire.[26] The resulting scattering spectrum shows fringes whose spacing is equal to the fringe spacing we measure experimentally, again allowing the group velocity to be extracted using eq 9. As shown in Figure 7, the calculated group velocities are in good agreement with the measured values.

Group velocities can also be determined from solutions to the waveguide model by numerical differentiation of $k_{SP}(\omega)$. Using the same diameters in the waveguide model that were used to obtain good agreement with measured propagation lengths (120 nm for the gold nanowires and 70 nm for the silver nanowires) also provides quantitative agreement with the measured group velocities. This confirms the validity of our interpretation of the fringes as arising from far-field interference. It also demonstrates that the group velocity, which is sensitive principally to the real part of the dielectric function, is not affected by errors in the tabulated values for the dielectric functions of the metals. (The reported experimental errors in ref 17 correspond to an error of less than 1% in the calculated group velocities.)

DISCUSSION

Approximating SP propagation using only the lowest-order waveguide mode in a solid metal cylinder provides quantitative agreement with the measured group velocities in both gold and silver nanowires and with the measured propagation lengths in gold nanowires. Disagreement between the model and measured propagation lengths in silver nanowires is attributable to inaccuracies in tabulated values of dielectric constants for silver. Our results thus indicate that a single waveguide mode dominates SP propagation in these nanowires. The ability to describe propagation using a single waveguide mode saves the computational effort that would otherwise be required for numerical simulations.

However, waveguide theory indicates that the nanowires considered here, with diameters close to 100 nm, should be able to support two or three waveguide modes.[31] The reason that the higher-order modes do not contribute to the measured propagation is not immediately clear. It may be that the symmetry of these modes is such that they are not efficiently excited by the incident light scattering off the input end of the nanowires. An additional possibility is that the higher-order waveguide modes are strongly damped, as compared to the fundamental mode, through radiation to the far field. The experimental methods used here will favor the observation of tightly confined modes that propagate efficiently to the far end of the wire and will not readily allow for the observation of leaky modes or other lossy modes. This is in contrast to previous measurements on larger-diameter silver nanowires that showed evidence of plasmons propagating in modes that were mostly confined to the corners of the pentagonal cross section.[32] In those earlier measurements, plasmon propagation was monitored by imaging light that leaks into a dielectric substrate from wires sitting at the dielectric–air interface; this imaging method favors the imaging of leaky modes, as evidenced by the short propagation lengths measured in these experiments.

We also note that we base our determination of group velocity on a different interpretation of the spectral fringes in the scattering spectra from the nanowires than in previous, similar studies.[11,12,33] In previous work, fringes in the output spectrum from silver nanowires were interpreted as arising from standing waves within the nanowires themselves. In order to form a standing wave, a propagating SP must interfere constructively with itself after propagating back and forth along the wire, over a total length $2L$. This is twice the length required for interference in our far-field model and thus leads to spectral fringes spaced half as far apart as the fringes that we observe experimentally. In ref 12, the measured fringe spacing is comparable to the spacing we measure; these fringes are interpreted as arising from standing waves, leading to a group velocity twice what we report for similar photon energies. Although it is difficult to make a direct comparison because of the different nanowire diameters, it seems possible that the fringes in ref 12 actually arose from far-field interference.

By comparison, the reported fringe spacings in refs 11 and 33 appear to be consistent with standing-wave resonances. In ref 11, at least, the nanowires were illuminated with an incoherent light source, unlike the coherent white-light continuum that we use. The incoherent source would prevent far-field interference between two points in the image. (Since it is unclear what illumination source is used in ref 33, we cannot comment further.) If the far-field interference has been removed, fringes due to the standing-wave resonances may then be resolved. These Fabry-Pérot fringes are expected to have lower visibility than the far-field fringes that we observe since the SPs will need to travel twice as far to produce this form of interference and will thus experience significantly stronger damping along the way. We believe that these Fabry-Pérot fringes still exist in our nanowire systems but are

obscured below the higher-visibility fringes that are associated with the far-field interference. We note also that illumination of the entire wire by a plane wave leads to excitation of only symmetric standing-wave modes, which would produce the same fringe spacing as in our measurements.[26,34] Our experimental configuration, with focused illumination of one end of long nanowires, is not subject to this symmetry consideration, so the same explanation cannot be used to explain our observed mode spacing.

It is also notable that this high fringe visibility measured experimentally (Figure 5a,b) is not reproduced in the simple model of far-field interference (Figure 6b,c). This model assumes that the scattering from the input end of the wire and the measured emission from the output end of the wire are both imaged as perfect, diffraction-limited spots onto the detector. The spectrum of scattered input light measured at the output arises from the wavelength dependence of the Airy disk pattern for a diffraction-limited spot, according to the first term on the right-hand side of eq 7. The spectrum of output light, by contrast, arises from the wavelength dependence of plasmon propagation losses along the wire. The relative contributions of input and output light thus vary with wavelength, leading to an interference pattern with relatively low visibility whose overall intensity varies nonmonotonically with wavelength. The shape of this interference pattern depends on the strength of scattering at the input end, as illustrated in Figure 6c.

The assumption of perfect, diffraction-limited spots is clearly an idealization of the real experimental situation, in which many factors contribute to broaden the spots in the image. For example, the excitation laser illuminates more than one point on the wire, so that scattering from the input end originates from a larger region than the point source considered in the model. In the calculation, we have assumed that light from the output area of the wire is collected over a fairly large spot size. In the experiment, the collection area may be smaller, which will lead to greater fringe visibility. In addition, the input end of the wire is located away from the center of the field of view of the microscope objective, so that spherical aberrations in the image are inevitable; these, together with chromatic aberrations in the imaging optics, will also serve to broaden the spot in the image corresponding to scattering off the input end of the wire. Furthermore, we have seen experimentally and theoretically that emission from the wire is not isotropic.[33] This has the effect of reducing the numerical aperture over which light is collected as compared to the full numerical aperture of the objective, which again broadens the output spot in the image; similar considerations are likely to apply to scattering at the input spot. Broadening of the spots in the image means that more scattered light from the input end of the wire will be collected when the output end of the wire is imaged, leading to greater fringe visibility. The non-idealities will also lead to a more uniform spectrum of scattered input light measured at the output end and thus to a more uniform interference pattern. The simplified case considered in the model thus represents the minimum amount of interference that could, in principle, be observed. The calculated far-field interference spectra should therefore not be taken to be a quantitative representation of the experimental spectra. Rather, they are meant to demonstrate that far-field interference leads to spectral fringes, even in an idealized situation, and that these fringes have the same spectral spacing as the fringes that are measured experimentally.

CONCLUSIONS

In summary, we measured propagation lengths and group velocities for surface plasmons propagating in chemically synthesized gold and silver nanowires. The experimental and theoretical results provide all the information necessary to use these nanowires as plasmonic interconnects in photonic circuits.

The propagation lengths are determined by imaging of two-photon fluorescence from dye molecules in the near field of the nanowires. The group velocities are determined by measuring the spectrum of light coming out one end of the wire when the opposite end is excited with a coherent white-light source. In these scattering measurements, the output spectrum exhibits fringes, which we interpret as being due to far-field interference between the output light and a small fraction of the incident light scattered off the input end of the wire. This is in contrast to previous experiments, where spectral fringes were interpreted as being produced by longitudinal standing waves in the wires.

The interpretation of far-field interference allows us to extract group velocities that are in quantitative agreement with rigorous numerical simulations based on the finite-difference time-domain method; these calculations also reproduce the measured propagation lengths in gold nanowires. Quantitative agreement with experimental values was also obtained using an analytical model that considers only the lowest-order waveguide mode in a solid metal cylinder, provided that the diameter of the waveguide is used as an adjustable parameter. Agreement between calculated and measured propagation lengths in silver nanowires is not very good, but the discrepancy can be explained as arising from inaccuracies in tabulated values for the dielectric function of silver.[17] The waveguide model thus demonstrates that plasmon propagation in the chemically synthesized nanowires is dominated by the lowest-order waveguide mode.

The results also indicate that plasmon propagation in the nanowires is dominated by the bulk dielectric functions of silver and gold, meaning that extrinsic

sources of loss such as scattering off surface roughness and grain boundaries are negligible. On the other hand, the intrinsic metal losses are still significant, particularly in the more chemically stable gold wires. Future work will therefore aim at overcoming these losses and further extending the propagation length by engineering the cross section of the wires and by coupling the surface plasmons to adjacent gain media.[35−38]

METHODS

Chemical Synthesis of Gold and Silver Nanowires. The gold nanowires were synthesized by tip-selective growth from gold nanorods at low pH.[14,15] First, purified gold nanorods with a high aspect ratio were synthesized using a method described in detail in ref 14. The length of these nanorods was increased by continuously adding a growth solution containing Au(I) ions and ascorbic acid. In this way, highly uniform and crystalline nanowires with pentagonal cross section and high aspect ratio were obtained.

The silver nanowires are synthesized following an established polyol process.[18,39] In a typical synthesis, 5 mL of ethylene glycol (J.T. Baker) was added to a 100 mL three-neck round flask. The solvent was heated at 160 °C for 1.5 h. Meanwhile, ethylene glycol solutions of 0.10 M $AgNO_3$ (Aldrich) and 0.15 M poly(vinyl pyrrolidone) (PVP, $M_W \approx 55\,000$, Aldrich, the concentration calculated in terms of the repeating unit) were prepared. To the PVP solution were added NaCl (Fisher) and tris-(acetylacetonato)iron(III) ($Fe(acac)_3$, Aldrich) in order to reach concentrations of 0.06 mM and 2.2 μM, respectively. In the next step, 3 mL of each solution (*i.e.*, $AgNO_3$ and PVP with additives) was simultaneously injected into the hot ethylene glycol with a syringe pump (KDS-200, KD Scientific Inc., Holliston, MA) at a rate of 45 mL/h. The reaction was maintained at 160 °C for additional 1.5 h. Magnetic stirring at 240 rpm was applied throughout the entire synthesis. This process results in high-quality crystalline wires with smooth surfaces, a pentagonal cross section, and very high aspect ratios.[40]

Sample Preparation. For deposition of gold nanowires, the nanowire solution, as synthesized, was diluted in water (1:10) and ~70 μL of the diluted solution was deposited on a glass coverslip and then dried in air at 70 °C for ~20 min. Excess surfactant that deposits on the substrate with the nanowires was washed off with methanol. For deposition of silver nanowires, the nanowire solution was diluted in ethanol (1:10) and ~10 μL of the diluted solution was deposited on a glass coverslip and then dried in air at room temperature for several minutes.

The samples were coated with a ~300 nm thick PMMA layer by spin coating a 4% solution of 950 kDa PMMA in anisole (MicroChem) at 6000 rpm and then baking for 60 s at 90 °C. For the propagation length measurements, 0.1 mM of Coumarin 30 (Sigma Aldrich) was dissolved into the PMMA solution before spin coating.

Measurement of Surface Plasmon Propagation Lengths. The sample was mounted on an inverted microscope (Olympus IX-71) and excited through a 40× objective (Olympus UPlanApo) by ultrafast laser pulses coming from a commercial tunable Ti:sapphire laser (Coherent Mira). The laser produces pulses with durations of approximately 1 ps and line widths of approximately 3 nm at a repetition rate of 76 MHz. The excited two-photon fluorescence was separated from the scattered laser light by a dichroic mirror and a short-pass filter and then imaged onto a CCD camera (PixelLink, PL-B957U). The polarization of the input laser was adjusted in order to maximize the fluorescence signal corresponding to plasmons propagating along the wire. For each registered image, the integration time was adjusted so that the bright spot at the end of the wire due to direct laser excitation is saturated but none of the image of the surface plasmon-excited emission along the wire is saturated. Twenty frames were averaged in order to form each image. The background level was determined by taking an average intensity at locations away from the wire and was subtracted from the measured signals. For each image, a line was drawn along the wire and the intensity cross section along that line was extracted as a function on the position of the nanowire. The scale of the image (micrometers per pixel) was calibrated using a standard U.S. Air Force resolution test chart. Measurements were made as a function of photon energy by tuning the excitation laser wavelength over the two-photon absorption range of the coumarin dye. The measurements were repeated for a different concentration of dye molecules (0.3 mM) in order to verify that direct absorption by the dye molecules is negligible.

Measurement of Surface Plasmon Group Velocities. The sample was mounted on an inverted microscope (Olympus IX-71) and light from a broad-band light source was focused by a long-working-distance microscope objective (Mitutoyo Plan Apo, 10×, NA = 0.28) through a glass prism onto one end of the nanowire. The polarization of the input light was adjusted in order to maximize the amount of light emerging from the far end of the wire. The white-light continuum was generated in a photonic-crystal fiber (Femtowhite 800, Newport), excited by a commercial Ti:sapphire laser (Coherent Micra). The light scattered from the output end of the nanowires was collected by a microscope objective (Olympus PlanApo, 40×, NA = 0.8) and was imaged onto the entrance slit of a grating spectrometer (Princeton Instruments SP 2300i). The light entering the spectrometer was dispersed spectrally and detected using a CCD camera (Andor Newton 920 BRD). A vertical row of pixels on the CCD detector was selected for data collection; together with the entrance slit on the spectrometer, this defines an area on the image from which light is collected and detected. The measured spectra were divided by the light that is scattered of the end of the nanowires in order to normalize spectral variance in the white-light continuum.

FDTD Simulations. For the FDTD simulations, we used the algorithm reported in ref 26. The grid size for all FDTD calculations was 4 nm. In these calculations, the complex, frequency-dependent dielectric constants for gold and silver were described by auxiliary differential equations[25] corresponding to a Drude plus two-pole Lorentzian model, with parameters chosen to be consistent with the tabulated values in ref 17 (unless indicated otherwise). The dielectric constant for the surrounding medium was $\varepsilon_S = 2.25$, corresponding to PMMA or glass. Gold nanowires with lengths of 10.5 μm and circular cross sections of 100 nm and silver nanowires with lengths of 6 μm and cross sections of 90 nm were simulated. These nanowire diameters were chosen to match the average diameters measured from SEM images.

Acknowledgment. Work at the Center for Nanoscale Materials was supported by the U.S. Department of Energy, Office of Science, Office of Basic Energy Sciences, under Contract No. DE-AC02-06CH11357. B.W. was supported by Deutsche Forschungsgemeinschaft (WI 3878/1-1). L.C. was partially supported by NSF CCI at UC Irvine (CHE-0616663). N.F.S. and S.K.G. acknowledges financial support from the NSF (CHE-1059057). E.R.Z. acknowledges financial support from the NSF (DMR-0547399, DMR-1105878) and the Robert A. Welch Foundation (C-1703). We thank Dr. Stephan Link for helpful discussions and Dr. Mason Guffey for assistance with SEM imaging.

REFERENCES AND NOTES

1. Barnes, W. L.; Dereux, A.; Ebbesen, T. W. Surface Plasmon Subwavelength Optics. *Nature* **2003**, *424*, 824–830.
2. Gramotnev, D. K.; Bozhevolnyi, S. I. Plasmonics Beyond the Diffraction Limit. *Nat. Photonics* **2010**, *4*, 83–91.
3. Takahara, J.; Yamagishi, S.; Taki, H.; Morimoto, A.; Kobayashi, T. Guiding of a One-Dimensional Optical Beam with Nanometer Diameter. *Opt. Lett.* **1997**, *22*, 475–477.

4. Weeber, J.-C.; Krenn, J. R.; Dereux, A.; Lamprecht, B.; Lacroute, Y.; Goudonnet, J. P. Near-Field Observation of Surface Plasmon Polariton Propagation on Thin Metal Stripes. *Phys. Rev. B* **2001**, *64*, 045411.
5. Zhou, Z.; Li, M; Yang, Z.; Peng, X.; Su, X.; Zhang, Z.; Li, J.; Kim, N.; Yu, X.; Zhou, L.; *et al.* Plasmon-Mediated Radiative Energy Transfer Across a Silver Nanowire Array *via* Resonant Transmission and Subwavelength Imaging. *ACS Nano* **2010**, *4*, 5003–5010.
6. Schider, G.; Krenn, J. R.; Hohenau, A.; Ditlbacher, H.; Leitner, A.; Aussenegg, F. R.; Schaich, W. L.; Puscasu, I.; Monacelli, B.; Boreman, G. Plasmon Dispersion Relation of Au and Ag Nanowires. *Phys. Rev. B* **2003**, *68*, 155427.
7. Gramotnev, D. K.; Pile, D. F. Single-Mode Subwavelength Waveguide with Channel Plasmon-Polaritons in Triangular Grooves on a Metal Surface. *Appl. Phys. Lett.* **2004**, *85*, 6323–6325.
8. Yatsui, T.; Kourogi, M.; Ohtsu, M. Plasmon Waveguide for Optical Far/Near-Field Conversion. *Appl. Phys. Lett.* **2001**, *79*, 4583.
9. Krenn, J. R.; Lamprecht, B.; Ditlbacher, H.; Schider, G.; Salerno, M.; Leitner, A.; Aussenegg, F. R. Non-diffraction-Limited Light Transport by Gold Nanowires. *EPL* **2002**, *60*, 663–669.
10. Verhagen, E.; Spasenovic, M.; Polman, A.; Kuipers, L. Nanowire Plasmon Excitation by Adiabatic Mode Transformation. *Phys. Rev. Lett.* **2009**, *102*, 203904.
11. Ditlbacher, H.; Hohenau, A.; Wagner, D.; Kreibig, U.; Rogers, M.; Hofer, F.; Aussenegg, F. R.; Krenn, J. R. Silver Nanowires as Surface Plasmon Resonators. *Phys. Rev. Lett.* **2005**, *95*, 257403.
12. Allione, M.; Temnov, V. V.; Fedutik, Y.; Woggon, U.; Artemyev, M. V. Surface Plasmon Mediated Interference Phenomena in Low-Q Silver Nanowire Cavities. *Nano Lett.* **2008**, *8*, 31–35.
13. Wiley, B. J.; Lipomi, D. J.; Bao, J.; Capasso, F.; Whitesides, G. M. Fabrication of Surface Plasmon Resonators by Nanoskiving Single-Crystalline Gold Microplates. *Nano Lett.* **2008**, *8*, 3023–3028.
14. Khanal, B. P.; Zubarev, E. R. Purification of High Aspect Ratio Gold Nanorods: Complete Removal of Platelets. *J. Am. Chem. Soc.* **2008**, *130*, 12634–12635.
15. Critchley, K.; Khanal, B. P; Gorzny, M. L.; Vigderman, L.; Evans, S. D.; Zubarev, E. R.; Kotov, N. A. Near-Bulk Conductivity of Gold Nanowires as Nanoscale Interconnects and the Role of Atomically Smooth Interface. *Adv. Mater.* **2010**, *22*, 2338–2342.
16. Solis, D.; Chang, W.; Khanal, B. P.; Bao, K.; Nordlander, P.; Zubarev, E. R.; Link, S. Bleach-Imaged Plasmon Propagation (BIPP) in Single Gold Nanowires. *Nano Lett.* **2010**, *10*, 3482–3485.
17. Johnson, P. B.; Christy, R. W. Optical Constants of the Noble Metals. *Phys. Rev. B* **1972**, *6*, 4370.
18. Sun, Y.; Gates, B.; Mayers, B.; Xia, Y. Crystalline Silver Nanowires by Soft Solution Processing. *Nano Lett.* **2002**, *2*, 165–168.
19. Ditlbacher, H.; Krenn, J. R.; Schider, G.; Leitner, A.; Aussenegg, F. R. Two-Dimensional Optics with Surface Plasmon Polaritons. *Appl. Phys. Lett.* **2002**, *81*, 1762–1764.
20. Shegai, T.; Huang, Y.; Xu, H.; Käll, M. Coloring Fluorescence Emission with Silver Nanowires. *Appl. Phys. Lett.* **2010**, *96*, 103114.
21. Sanders, A. W.; Routenberg, D. A.; Wiley, B. J.; Xia, Y.; Dufresne, E. R.; Reed, M. A. Observation of Plasmon Propagation, Redirection, and Fan-Out in Silver Nanowires. *Nano Lett.* **2006**, *6*, 1822–1826.
22. Yan, R.; Pausauskie, P.; Huang, J.; Yang, P. Direct Photonic-Plasmonic Coupling and Routing in Single Nanowires. *Proc. Natl. Acad. Sci. U.S.A.* **2009**, *106*, 21045–21050.
23. Ma, Y; Li, X.; Yu, H.; Tong, L.; Gu, Y.; Gong, Q. Direct Measurement of Propagation Losses in Silver Nanowires. *Opt. Lett.* **2010**, *35*, 1160–1162.
24. Nagpal, P.; Lindquist, N. C.; Oh, S.-H.; Norris, D. J. Ultrasmooth Patterned Metals for Plasmonics and Metamaterials. *Science* **2009**, *325*, 594–597.
25. Tavlove, A. *Computational Electrodynamics - The Finite Difference Time Domain Method*; Artech House: Norwood, MA, 1995.
26. Cao, L.; Nome, R. A.; Montgomery, J. M.; Gray, S. K.; Scherer, N. F. Controlling Plasmonic Wave Packets in Silver Nanowires. *Nano Lett.* **2010**, *10*, 3389–3394.
27. Stratton, J. A. *Electromagnetic Theory*; McGraw-Hill: New York, 1941.
28. Pfeiffer, C. A.; Economou, E. N.; Ngai, K. L. Surface Polaritons in a Circularly Cylindrical Interface: Surface Plasmons. *Phys. Rev. B* **1974**, *10*, 3038.
29. Press, W. H.; Flannery, B. P.; Teulkolsky, S. A.; Vetterling, W. T. *Numerical Recipes in Fortran 77: The Art of Scientific Computing*, 2nd ed.; Cambridge University Press: Cambridge, UK, 1992.
30. Palik, E. D. *Handbook of Optical Constants of Solids*; Academic Press: New York, 1985.
31. Prade, B.; Vinet, J. Y. Guided Optical Waves in Fibers with Negative Dielectric Constant. *J. Lightwave Technol.* **1995**, *12*, 6–18.
32. Song, M.; Bouhelier, A.; Bramant, P.; Sharma, J.; Dujardin, E.; Zhang, D.; Colas-des-Francs, G. Imaging Symmetry-Selected Corner Plasmon Modes in Penta-Twinned Crystalline Ag Nanowires. *ACS Nano* **2011**, *5*, 5874–5880.
33. Shegai, T.; Miljkovic, V.; Bao, K.; Xu, H.; Nordlander, P.; Johansson, P.; Käll, M. Unidirectional Broadband Light Emission from Supported Plasmonic Nanowires. *Nano Lett.* **2011**, *11*, 706–711.
34. Dorfmüller, J.; Vogelgesang, R.; Weitz, R. T.; Rockstuhl, C.; Etrich, C.; Pertsch, T.; Lederer, F.; Kern, K. Fabry-Pérot Resonances in One-Dimensional Plasmonic Nanostructures. *Nano Lett.* **2009**, *9*, 2372–2377.
35. Bergman, D. J.; Stockman, M. I. Surface Plasmon Amplification by Stimulated Emission of Radiation: Quantum Generation of Coherent Surface Plasmons in Nanosystems. *Phys. Rev. Lett.* **2003**, *90*, 027402.
36. Seidel, J.; Grafstroem, S.; Eng, L. Stimulated Emission of Surface Plasmons at the Interface between a Silver Film and an Optically Pumped Dye Solution. *Phys. Rev. Lett.* **2005**, *94*, 177401.
37. Noginov, M. A.; Zhu, G.; Mayy, M.; Ritzo, B. A.; Noginova, N.; Podolskiy, V. A. Stimulated Emission of Surface Plasmon Polaritons. *Phys. Rev. Lett.* **2008**, *101*, 226806.
38. Leon, I. D.; Berini, P. Amplification of Long-Range Surface Plasmons by a Dipolar Gain Medium. *Nat. Photonics* **2010**, *4*, 382–387.
39. Wiley, B.; Sun, Y.; Xia, Y. Polyol Synthesis of Silver Nanostructures: Control of Product Morphology with Fe(II) or Fe(III) Species. *Langmuir* **2005**, *21*, 8077–8080.
40. Sun, Y.; Mayers, B.; Herricks, T.; Xia, Y. Polyol Synthesis of Uniform Silver Nanowires: A Plausible Growth Mechanism and the Supporting Evidence. *Nano Lett.* **2003**, *3*, 955–960.